Plasma Chem Plasma Process (2016) 36:799–811
DOI 10.1007/s11090-016-9699-0

ORIGINAL PAPER

Synthesis, Characterization and Photocatalytic Application of TiO_2/SnO_2 Nanocomposite Obtained Under Non-thermal Plasma Condition at Atmospheric Pressure

Elie Acayanka[1] · Duclair S. kuete[1,2] · Georges Y. Kamgang[1] · Serge Nzali[3] · Samuel Laminsi[1] · Peter T. Ndifon[1]

Received: 16 December 2015 / Accepted: 7 March 2016 / Published online: 21 March 2016

Abstract A plasma-assisted synthesis of TiO_2/SnO_2 nanocomposite is described. In this approach, a precursor containing a mixture of [$TiCl_3$ and $SnCl_2$] exposed to electric discharge was oxidized by plasma-generated reactive species ($HO^{\cdot}/H_2O = 2.85$ eV/SHE). SnO_2 microstructures with a diameter of 10–40 μm were coated by thin layers TiO_2 nanorods with mean diameter of 6–8 nm. The obtained TiO_2/SnO_2 nanocomposite was characterized by transmission and scanning electron microscopy, X-ray diffraction and Fourier transform infrared. TiO_2/SnO_2 nanocomposite was found to be a promising new material for the photocatalytic discoloration of aqueous Remazol Brilliant Blue-R dye under daylight and UVA light sources, due to the combined effects of large specific surface area and heterojunction which efficiently separates the electron–hole pairs delaying the charge recombination. The leaching test indicated that the nanocomposite is stable easily reusable.

Keywords Non-thermal plasma · TiO_2/SnO_2 · Nanocomposite · Photocatalysis · Remazol Brilliant Blue R dye

✉ Elie Acayanka
acayanka@gmail.com

✉ Samuel Laminsi
slaminsi@uy1.uninet.cm

[1] Department of Inorganic Chemistry, Faculty of Science, University of Yaounde I, P.O. Box 812, Yaoundé, Cameroon

[2] Department of Chemistry and Physics of Solids and Surfaces, Institut Jean Lamour, Parc de Saurupt, CS 50840, 54011 Nancy Cedex, France

[3] Faculty of Agronomy and Agricultural Sciences, School of Wood, Water and Natural Resources, University of Dschang, Ebolowa Campus, P.O. Box 786, Ebolowa, Cameroon

Introduction

The development of efficient photocatalysts has become a crucial issue in order to address the problem of pollution from textile and food industries. Particularly in the case of textiles, about 10–60 % of dyes are lost during the manufacturing process, resulting in large amounts of highly coloured wastewater [1]. Such coloured waters in the ecosystem are source of aesthetic pollution causing perturbation to aquatic life [2]. Moreover, these dyes are toxic, mutagenic and carcinogenic, so their removal is highly required [3–5]. Many techniques of water treatment exist. Some biological and physicochemical treatments are expensive and bulky. This has led many scientists to propose alternatives techniques such as transferring the pollutant from aqueous phase to solid phase e.g.: adsorption, coagulation and precipitation which have been longer satisfactory. But, due to the exponential increase in the amount and the complexity of pollutants, the formed sludge treatment became a more complex challenge and therefore, these techniques have become ineffective. Hence, other strategies have to be developed in order to reduce the water pollution.

Recently, advanced oxidation processes (AOPs) have been widely investigated [6–8]. AOPs are based on the generation of non-selective oxidizing agent: the hydroxyl radical $OH^{\cdot}$. This radical can be produced by heterogeneous catalytic oxidation processes; photo-Fenton processes and/or electric discharges techniques operating at/or near ambient temperature and pressure [9]. Among the heterogeneous photocatalyst materials usually applicable to environmental remediation, a special attention has been focused on wide variety of TiO_2 particles with particular emphasis pointed towards their optical response shifted to the visible spectrum of solar radiation [10–12]. Despite several advances in this domain, it is still difficult to find a photocatalyst that is efficient, stable, reusable, cost-effective and environmental friendly. Moreover, handling nanoscale particles in water depollution is a crucial problem because it is often expensive to separate TiO_2 nanomaterials of treated wastewater and the nanoparticles are generally found in the environment or in biological systems. Thus, to overcome these problems, the developments of new heterojunctions either by incorporating secondary semiconductor metal or carbon quantum dots nanoparticles are some major strategies implemented [13, 14].

In the present work, tin oxide (SnO_2), which is widely studied n-type semiconductor, is used as catalyst supports for TiO_2 nanoparticles thanks to the plasma-assisted approach. The obtained composites could provide considerable advantages such as, easier solid–liquid separation and good dispersion. Also, the coupling of different semiconductors with desirable matching of their electronic band structures could suppress or delay as far as possible the recombination of the photogenerated charge carriers (electrons and holes), that is the main limitation in the efficiency of any photocatalytic process [15, 16]. In addition, the modification of material properties, such as particle size, surface area, porosity and crystallinity are some key parameters expected by this method in order to achieve high efficiency. In this regards, we recently reported the effectiveness of a Gliding arc plasma method for synthesis of nanocrystalline titania involving oxidation of $TiCl_3$ [17]. The obtained rod-shaped nanoparticles showed higher activity attributed to their larger surface-to-volume ratio which enhances the contact between pollutant and catalyst. However their effective use still suffers from numerous drawbacks such as facile agglomeration which impedes their consistent distributions. Following the same approach, the present work concerns a particular type of plasma discharge—the gliding discharge or "Glidarc" which operates at atmospheric pressure and belongs to the family of non-thermal plasmas. The

gliding arc technique was firstly introduced for gas treatments several decades ago by Czernichowski et al. [18, 19], and later developed to liquid treatments [20–24]. The flux of the plasma activated species is governed by the gas composition. For the discharges in moist air, Benstaali et al. [25] showed that the major species were radicals $HO^{\cdot}$ and $NO^{\cdot}$. The main chemical properties expected for a gliding arc treatment, are oxidizing and acidifying effects [23, 26–28].

The photocatalytic efficiency of synthesized TiO_2/SnO_2 composite was evaluated by studying the discoloration of Remazol Brilliant Blue-R dye (RBB-R). The RBB-R was selected as representative dye in textile industry, widely used for its lively and bright colour.

Experimental Procedure

Plasma Reactor for Synthesis of TiO_2/SnO_2

The gliding arc system used for this study was described elsewhere [23]. The Fig. 1 shows the overall scheme of the experimental setup. We are concerned with a particular type of discharge—the gliding discharge or "glidarc" which burns at atmospheric pressure and belongs to the family of the non-thermal plasmas. The reactor body is made of a glass cylindrical vessel with a volume of approximately 1 L. The chamber length is H = 22.5 cm and the diameter is d = 10.5 cm.

The feeding gas was water-saturated air, provided by a compressor and passing through a bubbling flask before entering the reactor. The experiments were conducted at a gas flow rate of 800 L/h. Water–air was sprayed directly into the reactor through an atomizing nozzle. The nozzle diameter is e = 25 mm around which are disposed symmetrically two metal electrodes with diverging profile.

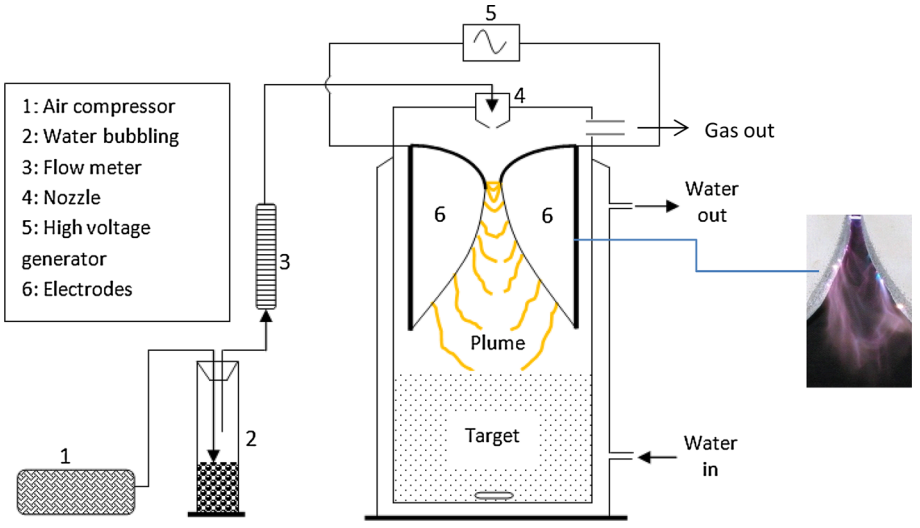

Fig. 1 Experimental set-up involving a high voltage transformer (HV = 10 kV/1 A); electrode distance to target d = 2.5 cm. Gas flow rate: 800 L h^{-1}

The electrodes are connected to an AC 220 V/10 kV–1 A high voltage transformer which delivers a mean current intensity 160 mA (600 V/P # 100 W). In the operating condition, an electric arc occurs at the minimum spacing between electrodes and glides over the latter, thus generating excited species and free radicals which confer particular chemical properties to the plasma. The thermal energy available in the arc enables the energy transfer to the "parent species", and thus favours the breaking of H–OH and O=O bonds. This feature requires less energy than $N \equiv N$ breaking and allows the transition of gaseous moieties from their fundamental energy level to the excited energy level. This plume of soaked plasma licks a target solution ($SnCl_2 + TiCl_3$) placed on the axis of the reactor at a distance of about 2.5 cm.

Plasma Chemistry

In humid air, the discharge is known to induce acidifying and oxidizing effects in an aqueous target solution. The main primary species $HO^{\cdot}$ and $NO^{\cdot}$ radicals, mainly formed in the arc will be the determining agents for the chemical reactions observed in the target solution. The formation of $HO^{\cdot}$ and $NO^{\cdot}$ as the main products is confirmed by spectroscopy measurements and results from electron impact on water [25]. The radical $HO^{\cdot}$ is very reactive [E° ($HO^{\cdot}/H_2O$) = 2.85 V/SHE] with a lifetime of a hundred nanoseconds [29]. Hence the assumption of the formation of the dimer H_2O_2 is quite reasonable and may take place in the gas phase or at the liquid surface. H_2O_2 is water soluble [$E^{\circ}(H_2O_2/H_2O)$ = 1.76 V/SHE] and may diffuse in the solution and later react with solutes. The formation of $NO^{\cdot}$ induces the acidifying property which is in agreement with the Birkeland process. $NO^{\cdot}$ enters a series of complex reactions leading to the formation of nitric acid via unstable nitrous acid and peroxynitrite [27, 28].

The $HO^{\cdot}$ radicals result from electron impact on water according to Eqs. 1 and 2 [25].

$$H_2O + e^- \rightarrow OH^{\cdot} + H^{\cdot} + e^- \quad (1)$$

$$H_2O + e^- \rightarrow OH^{\cdot} + H^+ + 2e^- \quad (2)$$

Therefore, the following reactions are expected to take place:

$$\textbf{Oxidation}: \quad TiCl_3 + 2H_2O \rightarrow TiO_2 + 3Cl^- + 4H^+ + e^- \quad E = -0.67\,V \quad (3)$$

$$SnCl_2 + 2H_2O \rightarrow SnO_2 + 2Cl^- + 4H^+ + 2e^- \quad E = 0.094\,V \quad (4)$$

$$\textbf{Reduction}: \quad OH^{\cdot} + H^+ + e^- \rightarrow H_2O \quad E = 2.85\,V \quad (5)$$

$$\textbf{Balance}: \quad TiCl_3 + SnCl_2 + 3OH^{\cdot} + H_2O \rightarrow TiO_2/SnO_2 + 5HCl \quad (6)$$

This is an essential feature which confirms previous observations on the plasma-chemical properties of the gliding discharge relevant to the oxidizing degradation of organic wastes [30–36].

Synthesis of TiO_2/SnO_2 Nanocomposite

All chemicals were of analytical grade obtained from commercial sources and used as purchased. The $SnCl_2$ solution (2 mol L^{-1}) was prepared by dissolving in de-ionized water a sample of Tin (II) chloride dihydrate $SnCl_2.2H_2O$ weighed using a Sartorius balance with accuracy of 1/10000. Subsequently, the $TiCl_3$ solution (2 mol L^{-1}) was prepared by

diluting the commercial stock solution. The working sample used as precursor was obtained by mixing the both [$TiCl_3$ and $SnCl_2$] solutions in a 50:50 (v/v) ratio. For these experiments, 450 mL was poured slowly into a water cooled glass reactor (Fig. 1) at a distance of about 2.5 cm from the electrodes tips. The solution was magnetically stirred and was exposed to the plasma for t* = 30 min following the previous work of Acayanka et al. [17]. After the discharge was switched-off, the exposed solution was cooled at room temperature and centrifuged at 3600 rpm for 10 min; the resulting TiO_2/SnO_2 precipitate was washed several times with deionised water and dried at ambient laboratory condition.

Analytical Methods

The morphology of obtained TiO_2/SnO_2 nanocomposite was analyzed with a Scanning Electron Microscopy, Philips XL 30 FEG (Field Emission Gun) using an acceleration voltage of 5 kV. XRD-pattern of the powder was obtained using a Bruker D8 diffractometer equipped with CuKα radiation (1.5406 Å). The patterns were recorded during 20 h for 2θ values between 20° and 80° at a scanning step of 0.02°. The ICDD-JCPDS database was used to identify the crystalline phases. Transmission electron micrographs were obtained using a Tecnai F30 microscope (field emission cathode) with an acceleration voltage of 300 kV. The FTIR spectrum was recorded in total reflectance mode using a KBr pellet containing 0.5 % of sample. The spectrum is obtained as an accumulation of 16 scans with 2 cm^{-1} step.

Photocatalytic Study

The photocatalytic studies are used to follow-up the discoloration efficiency of the synthesized TiO_2/SnO_2 nanocomposite and were performed on aqueous Remazol Brilliant Blue-R (RBB-R) dye using batch contact method. The chemical structure of RBB-R dye is given in Fig. 2. For these experiments two types of treatments were considered. First, exposure to plasma irradiation of a mixture solution containing 1.0 g of photocatalyst incorporated into 450 mL of RBB-R dye (50 mol L^{-1}); while a control experiment in the absence of photocatalyst under plasma irradiation was also performed in order to determine the contribution of generated species. Secondly, exposure to daylight irradiation of a mixture solution containing 1.0 g of photocatalyst incorporated into 450 mL of RBB-R dye solution (50 mol L^{-1}) in a beaker. The sunlight experiments were conducted in June

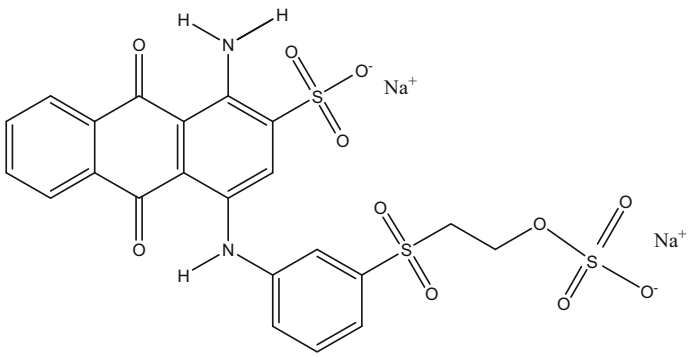

Fig. 2 Scheme of molecular Remazol Brilliant Blue-R (RBB-R) dye

2015 (10 a.m. to 3 p.m.), when the fluctuation of the sunlight intensity is minimal. The average daylight intensity of 4 kWh m^{-2} day^{-1} was measured by digital lux meter with errors of 5 %. All these solutions were previously magnetically stirred in the absence of light for 10 min to establish the adsorption–desorption equilibrium. At given intervals, an aliquot of exposed solution was withdrawn and centrifuged at 3600 rpm for 5 min, the obtained supernatant was immediately analysed using a JENWAY UV–Vis spectrophotometer. The absorbance measurements were made in triplicate at the maximum wavelength of RBB-R dye at 594 nm (λ_{max}). The discoloration efficiency of the prepared nanocomposite was determined by Eq. (7).

$$Discoloration\ efficiency\ (\%) = 100 \cdot \frac{C_0 - C_t}{C_0} \tag{7}$$

where C_o is the initial dye concentration (mg L^{-1}), and C_t is the dye concentration (mg L^{-1}) at reaction time, t (min).

Leaching Tests

The chemical stability of the nanocomposite was assessed using potential leaching of active species. For this purpose, 1.0 g of photocatalyst incorporated into 450 mL of RBB-R dye solution (50 mol L^{-1}) were introduced in a beaker and the mixture was exposed to daylight and plasma condition. After 10 min of irradiation, part of the reaction mixture was filtered and the supernatant was carefully investigated under the same photocatalytic conditions in order to see if the active particles are detached in solution.

Results and Discussion

Characterization of Obtained TiO_2/SnO_2

X-ray Analysis

The X-ray diffraction patterns (XRD) of the TiO_2 nanostructure, SnO_2 particle and the TiO_2/SnO_2 nanocomposite are respectively depicted on Fig. 3a–c. As can be seen, the peaks at 2θ values of 27.20° (110), 36.88° (101), 53.12° (211), 54.64° (220) and 62.72° (310) on Fig. 3c, confirm the presence of tin oxide (SnO_2) in accordance with the standard values (ICDD card no 04-006-9484). Meanwhile the peaks at 2θ values around 27.60°, 40.43°, 44.07°, 53.67° and 68.61° represent (110), (111), (210), (211) and (301) set of lattice planes of TiO_2 (ICDD card no 21-1276). These observations are better corroborated by comparing the Fig. 3c both to the spectra of TiO_2 alone (Fig. 3a) and SnO_2 alone (Fig. 3b). As a result, the two peaks (101) and (310) respectively at 36.88° and 62.72° assigned to tin oxide (SnO_2) are obviously not present on Fig. 3a and thereby show the aforementioned oxi- precipitation of Ti(III) and Sn(II) chlorides into TiO_2/SnO_2 composite. It also should be highlighted that, the TiO_2 nanostructure consist of both anatase and rutile phases. Despite the fact that anatase TiO_2 is a more efficient photocatalyst than the rutile TiO_2, it was shown that mixture of the two phases exhibit much superior photocatalytic activity than each pure phase [37]. This crystallinity coupled to heterojunction between TiO_2 and SnO_2 will promote the separation of photogenerated electrons and holes. Thus, the synthesized nanocomposite should exhibit greater efficiency.

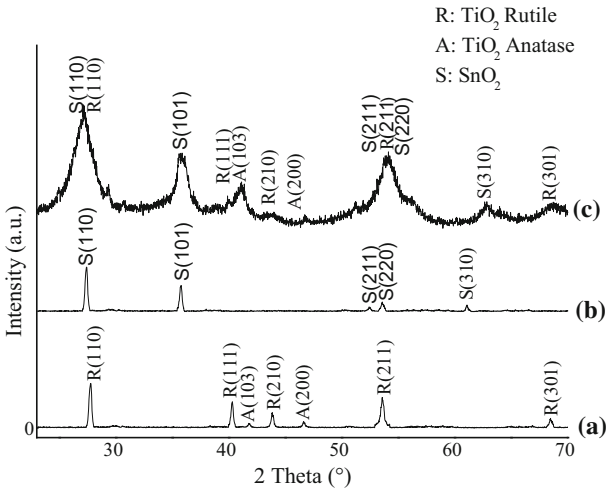

Fig. 3 *a* X-ray diffraction patterns of TiO_2 nanostructure. (*b*) X-ray diffraction patterns of SnO_2 microstructure. *c* X-ray diffraction patterns of TiO_2/SnO_2 nanocomposite

Morphological Properties

Figure 4 shows the SEM micrograph of the synthesized SnO_2 microparticles under plasma at atmospheric pressure after 30 min of exposure. Micrograph in Fig. 4b is a magnification of area on Fig. 4a obtained for the plasma irradiation of $SnCl_2$ (450 mL, 2 mol L^{-1}) alone. The resulting SnO_2 with cubic microstructures (10–40 µm) can be seen. Figure 4c, d presents the SEM pictures of synthesized TiO_2 obtained from precursor $TiCl_3$ alone. These micrographs show that the morphology of the particles consists of anisotropic rods and the particles are not compacts which could allow the diffusion of pollutants and their better dispersion.

Figure 4c shows the SEM surface morphologies of the TiO_2/SnO_2 nanocomposite. On the higher magnification (Fig. 4d), it is observed that SnO_2 microparticles are completely coated with TiO_2 nanorods in comparison with the SEM micrograph on Fig. 4b. This result is confirmed by the TEM micrograph of Fig. 5b on which we can observe the nanorods of TiO_2 with a mean diameter of 6–8 nm. The position of TiO_2 nanorods is depicted by the dotted line on Fig. 5a. This position is obtained by scratching the surface with a diamond tip and the material is transferred on a TEM copper grid.

Considering that the photocatalytic reactions occur on the surface of semiconductor materials, the efficiency therefore greatly depends on particle morphology. From results presented, the use of SnO_2 as a support is a great strategy to achieve a higher dispersion of TiO_2 and increase the specific surface area. In general, interface properties can be attributed to two important aspects: the lattice match between the two components and the suitable valence and conduction band levels. However, in our case, the observed size difference and the kinetic formation are probably the key features to consider. FESEM analysis shows that the SnO_2 particles are in tens of micron size and TiO_2 are of nano size, it is then quite reasonable that the SnO_2 which is denser become completely coated with TiO_2 nanorods.

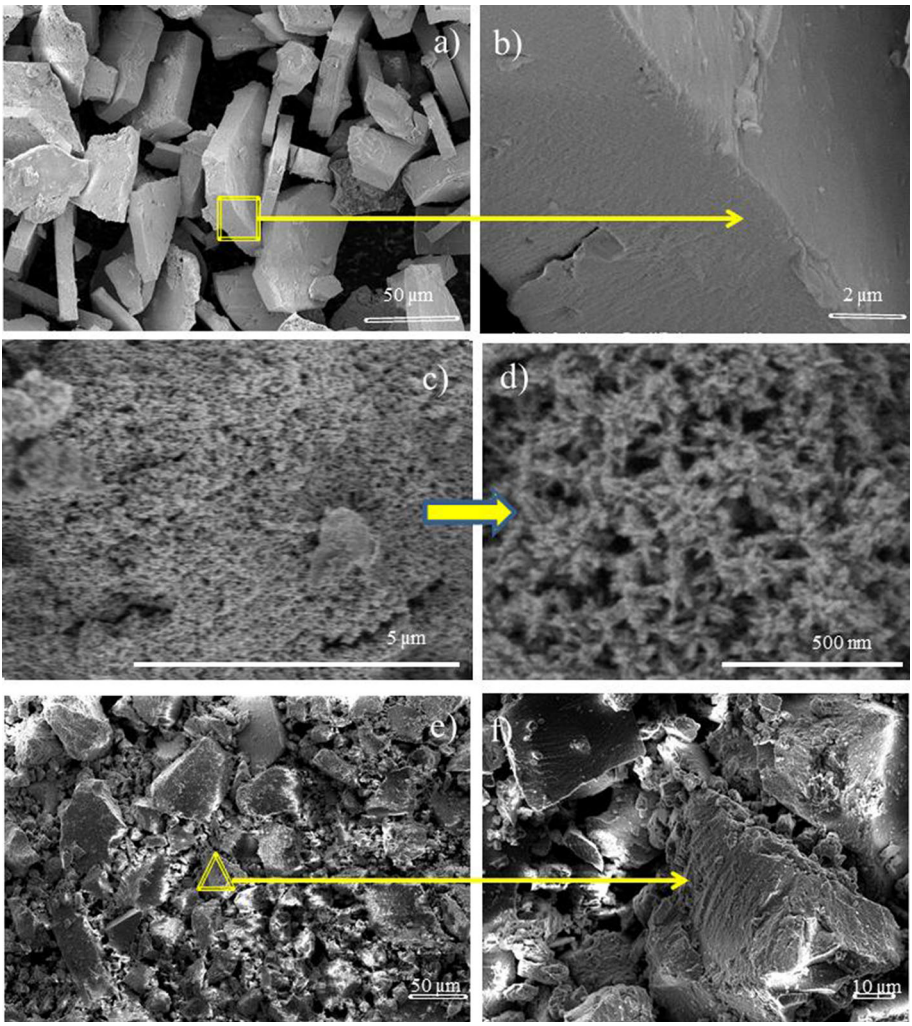

Fig. 4 **a** SEM micrograph of synthesized SnO_2 microparticles obtained by exposing a solution of $SnCl_2$ alone under plasma at atmospheric pressure after 30 min. **b** Magnification of a square area of Fig. 4a. **c**, **d** SEM micrograph at different magnifications of synthesized TiO_2 particles obtained by exposing a solution of $TiCl_3$ alone under plasma at atmospheric pressure after 30 min. **e** SEM surface morphologies of the TiO_2/SnO_2 nanocomposite prepared by exposing to the plasma a mixture of $SnCl_2$ and $TiCl_3$ solution after 30 min. **f** Surface morphology of TiO_2/SnO_2 at high magnification

Infrared Spectroscopy

The FTIR spectrum of TiO_2/SnO_2 nanocomposite is shown in Fig. 6. The broad band at 3230 cm^{-1} is associated with the characteristic vibrational mode of the OH groups of adsorbed water. The peak at 1605 cm^{-1} is assigned to the bending vibrations of surface-adsorbed molecular water. The absorption broad band between [600–620 cm^{-1}] correspond both to (Ti–O and Ti–O–Ti) stretching vibrations [38, 39] and to (Sn–O and Sn–O–

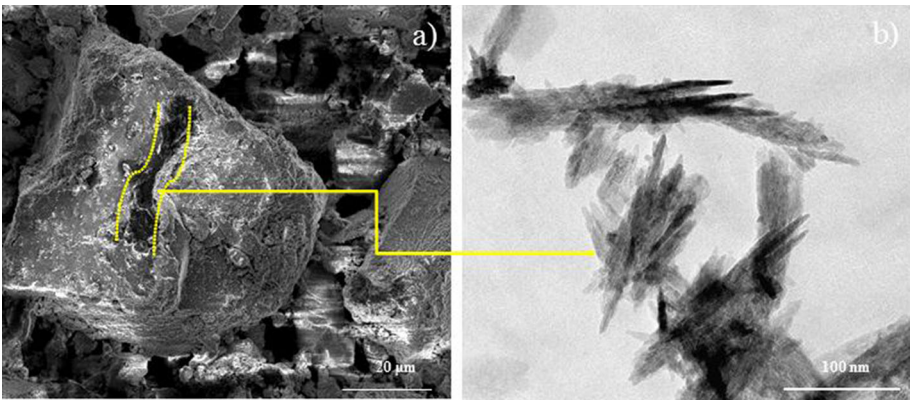

Fig. 5 **a** SEM micrograph of synthesized TiO_2/SnO_2 nanocomposites under plasma at atmospheric pressure after 30 min. **b** TEM micrograph of TiO_2 nanorods

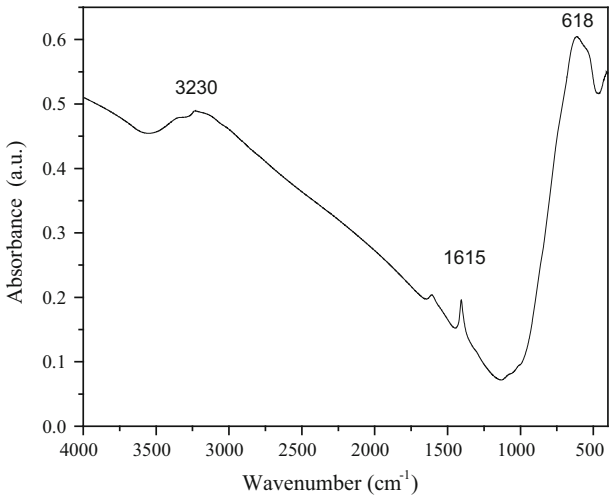

Fig. 6 FTIR spectrum of TiO_2/SnO_2 nanocomposite

Sn) stretching [40, 41]. The presence of these bands confirms that TiO_2/SnO_2 nanocomposite is formed.

Photocatalytic Discoloration of Remazol Brilliant Blue R Dye (RBB-R) by TiO_2/SnO_2 Nanocomposite

The photocatalytic activity of TiO_2/SnO_2 nanocomposite was evaluated by photo-discoloration of RBB-R dye solution under daylight and plasma irradiation. The UV–Vis spectra were recorded from 250 to 800 nm. The results are shown in Fig. 7a for plasma irradiation and in Fig. 7b for daylight. As can be seen, whatever the radiation source, the spectra show a significant peak decrease at 594 nm (corresponding to the maximum wavelength of dye

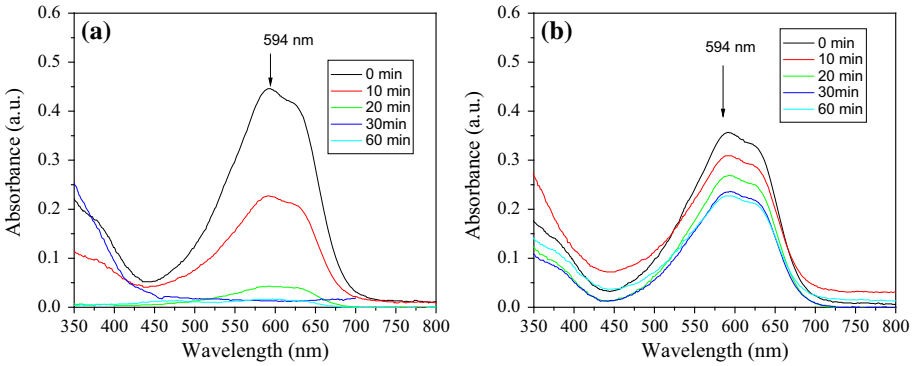

Fig. 7 Evolution of the absorbance spectra of Remazol Brilliant Blue R (RBB-R) exposed to **a** the plasma discharge and **b** the sunlight irradiation, for t* = 0, 10, 20, 30 and 60 min at 594 nm

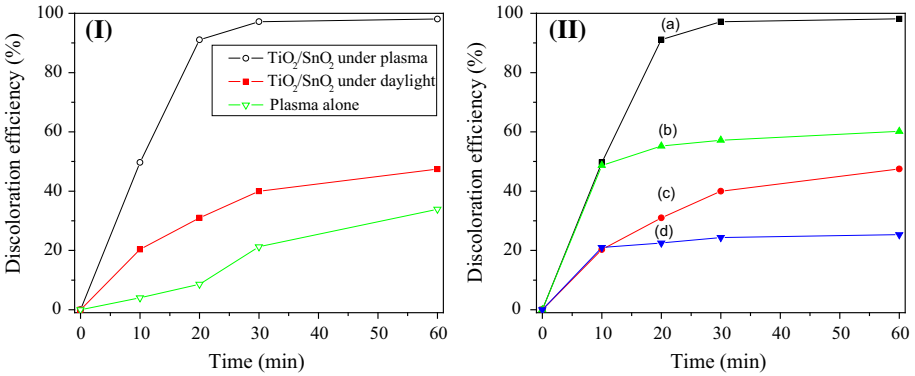

Fig. 8 Evolution of RBB-R discoloration efficiency (**I**) and catalyst dependence (**II**) (*a*-standard experiment under plasma, *b*-leaching test under plasma irradiation, *c*-standard experiment under daylight and *d*-leaching test under daylight irradiation)

RBB-R). The corresponding discoloration rates showed on Fig. 8(I) are 47.45 % for daylight irradiation and 98.09 % for plasma irradiation. In addition, the discoloration efficiency for plasma alone without a catalyst is 33.91 %. These results clearly highlight the efficiency of the obtained TiO_2/SnO_2 nanocomposite. The analysis of these results requires some comments: (1) In the case of plasma alone without catalyst, a slight color decrease is in good agreement with previous results relating the exposure of organic compounds [30–36, 42]. This is due to the oxidation of RBB-R dye by the primary entities $HO^{\cdot}$ created in the discharge and to the formation of secondary species soluble in water such as H_2O_2. The main problem in this case remains the increase of efficiency and the decrease of exposure time aiming to reduce the energy cost of treatment. (2) In the case of daylight and plasma irradiation, the significant discoloration efficiency was attributed to the nanoscale size of TiO_2 which causes their good dispersion on the surface of SnO_2 and enhances the efficiency. The satisfactory results in the case of plasma irradiation are due to additional hydroxyl radicals $OH^{\cdot}$, formed in gaseous discharges and to UV light emitted by

the discharge that enhances the formation of excited particles and promotes the dissociation of adsorbed water molecules according to Eqs. 8 and 9:

$$TiO_2 + h\nu \rightarrow e^- + h^+ \quad (8)$$

$$H_2O + h^+ \rightarrow OH^{\cdot} + H^+ \quad (9)$$

where h^+ refers to a positive hole.

The remarkably photocatalytic performance of TiO_2/SnO_2 nanocomposites, was compared with other recent reports related to the combination of photocatalysts with non-thermal plasma technique. For instance, α-FeOOH exhibits 73 % for Orange II bleaching after 120 min of plasma irradiation [36]; the Degussa P25 TiO_2-attained 80 % for the discoloration of acid orange 7 after 30 min of plasma irradiation [43]. The incorporation of maghemite (γ-Fe_2O_3) increases the discoloration rate under plasma up to 55.6 % after 60 min [34]. Similarly, the discoloration AG25 anthraquinone dye gives 50 % after 120 min in the presence of thin layer of TiO_2 [44]. Therefore, we could conclude that the synthesized TiO_2/SnO_2 nanocomposite (with photocatalytic activity of 98.09 % under plasma irradiation for the discoloration of RBB-R dye) is a promising nanomaterial with high potential for photocatalytic applications.

Catalyst Stability and Leaching Test

The photostability of the synthesized TiO_2/SnO_2 nanocomposite was examined by investigating its leaching behavior under daylight and plasma irradiation. The test consists in removing the catalyst from treated solution and to follow the behavior of supernatant. As a result, no significant photocatalytic activity was noted on Fig. 8(II) after the catalyst is withdrawn. This indicates that the TiO_2 nanorods are tightly bound on the surface of the SnO_2 through electrostatic interactions, and a strong hetero/junction formed between the TiO_2 and SnO_2. Thus, developing semiconductor by combining two different catalysts is a powerful strategy for improving the separation efficiency.

Conclusion

The results presented in this work indicate that the gliding arc plasma discharges can be effectively used for the synthesis of TiO_2/SnO_2 nanocomposite. Due to the high reactivity of produced species ($HO^{\cdot}/H_2O$) when the electric discharges take place in moist air as a feeding gas, the TiO_2/SnO_2 nanocomposite is obtained simply by the oxi-precipitation of precursor ($TiCl_3$ + $SnCl_2$) without any other reagents added. This feature gives the possibility to synthesize a high purity photocatalyst through a simple approach. Furthermore, the synthesized TiO_2/SnO_2 nanocomposite exhibited excellent photocatalytic activity for the discoloration of Remazol Brilliant Blue-R (RBB-R) dye, with a percentage of 47.45 % under daylight and 98.09 % under plasma irradiation. In addition, it was found that whatever the nature of radiation, the contact time had no major influence on the leached amount.

Acknowledgments The authors are grateful to the International Foundation for Sciences (IFS) for a JENWAY spectrophotometer offered to S.N., Special thanks are also addressed to the emeritus Professor Jean-Louis Brisset of Rouen University (France) for a Plasma reactor support and to the professor Eder C. Lima of Federal University of Rio Grande do Sul—UFRGS (Brazil) for some of the reagents used in this work.

References

1. Hessel C, Allegre C, Maisseu M, Charbit F, Moulin P (2007) Guidelines and legislation for dye house effluents. J Environ Manage 83:171–180
2. da Silva LG, Ruggiero R, Gontijo PM, Pinto RB, Royer B, Lima EC, Fernandes THM, Calvete T (2011) Adsorption of Brilliant Red 2BE dye from water solutions by a chemically modified sugarcane bagasse lignin. Chem Eng J 168:620–628
3. Cardoso NF, Lima EC, Royer B, Bach MV, Dotto GL, Pinto LAA, Calvete T (2012) Comparison of *Spirulina platensis* microalgae and commercial activated carbon as adsorbents for the removal of Reactive Red 120 dye from aqueous effluents. J Hazard Mater 241–242:146–153
4. Royer B, Cardoso NF, Lima EC, Macedo TR, Airoldi C (2010) A useful organofunctionalized layered silicate for textile dye removal. J Hazard Mater 181:366–374
5. Carneiro PA, Umbuzeiro GA, Oliveira DP, Zanoni MVB (2010) Assessment of water contamination caused by a mutagenic textile effluent/dyehouse effluent bearing disperse dyes. J Hazard Mater 174:694–699
6. Kariyajjanavar P, Narayana J, Arthoba Nayaka Y (2013) Degradation of textile dye C.I. Vat Black 27 by electrochemical method by using carbon electrodes. J Environ Chem Eng 1:975–980
7. Liu Y, Tian H, Si A (2012) Gliding arc discharge for decolorization and biodegradability of azo dyes and printing and dyeing wastewater. Plasma Chem Plasma Process 32:597–607
8. Peng J, Lee S (2013) Atmospheric pressure plasma degradation of azo dyes in water: pH and structural effects. Plasma Chem Plasma Process 33:1063–1072
9. Babuponnusami A, Muthukumar K (2014) A review on Fenton and improvements to the Fenton process for wastewater treatment. J Environ Chem Eng 2:557–572
10. Waseem Raz MM, Haque M, Muneer M, Fleisch A, Hakki D (2015) Bahnemann, Photocatalytic degradation of different chromophoric dyes in aqueous phase using La and Mo doped TiO_2 hybrid carbon spheres. J Alloys Compd 632:837–844
11. Qamar M, Merzougui B, Anjum D, Hakeem AS, Yamani ZH, Bahnemann D (2014) Synthesis and photocatalytic activity of mesoporous nanocrystalline Fe-doped titanium dioxide. Catal Today 230:158–165
12. Manassero A, Satuf ML, Alfano OM (2013) Evaluation of UV and visible light activity of TiO_2 catalysts for water remediation. Chem Eng J 225:378–386
13. Suryawanshi A, Dhanasekaran P, Mhamane D, Kelkar S, Patil S, Gupta N et al (2012) Doubling of photocatalytic H_2 evolution from g-C_3N_4 via its nanocomposite formation with multiwall carbon nanotubes: electronic and morphological effects. Int J Hydrogen Energy 37:9584–9589
14. Cheng N, Tian J, Liu Q, Ge C, Qusti AH, Asiri AM et al (2013) Au-nanoparticle loaded graphitic carbon nitride nanosheets: green photocatalytic synthesis and application toward the degradation of organic pollutants. ACS Appl Mater Interfaces 5:6815–6819
15. Ismail AA, Bahnemann DW, Al-Sayari SA (2012) Synthesis and photocatalytic properties of nanocrystalline Au, Pd and Pt photodeposited onto mesoporous RuO_2–TiO_2 nanocomposites. Appl Catal A Gen 431–432:62–68
16. Chun H, Yizhong W, Hongxiao T (2001) Preparation and characterization of surface bond-conjugated TiO_2/SiO_2 and photocatalysis for azo dyes. Appl Catal B Environ 30:277–285
17. Acayanka E, Tiya Djowe A, Laminsi S, Tchoumkwe CC, Nzali S, Poupi Mbouopda A, Ndifon PT, Gaigneaux EM (2013) Plasma-assisted synthesis of TiO_2 nanorods by gliding arc discharge processing at atmospheric pressure for photocatalytic applications. Plasma Chem Plasma Process 33:725–735
18. Czernichowski A (1994) Gliding arc: application to engineering and environmental control. Pure Appl Chem 66:1301–1310
19. Fridman AA, Petrousov A, Chapelle J, Cornier JM, Czernichowski A, Lessueur H, Stevefelt J (1994) Modèle physique de l'arc glissant. J Phys III 4:1449–1465
20. Benstaali B, Moussa D, Addou A, Brisset JL (1998) Plasma treatment of aqueous solutes: some chemical properties of gliding arc in humid air. Eur Phys J Appl Phys 4:171–179
21. Brethes-Dupouey S, Peyrous R, Held B (2000) Removal of H_2S in air by using gliding arc discharges. Eur Phys J Appl Phys 11:43–58
22. Abdelmalek FS, Gharbi S, Benstaali B, Addou A, Brisset JL (2004) Plasmachemical degradation of azo dyes by humid air plasma: yellow supranol 4 GL, scarlet red nylosan F3 GL and industrial waste. Water Res 38:2339–2347
23. Burlica R, Kirpatrick MJ, Locke BR (2006) Formation of reactive species in gliding arc discharges with liquid water. J Electrostat 64:35–43

24. Doubla A, Laminsi S, Nzali S, Njoyin E, Kamsu-kom J, Brisset JL (2007) Organic pollutants abatement and biodecontamination of brewry effluents by a non-thermal quenched plasma at atmospheric pressure. Chemosphere 69:332–337
25. Benstaali B, Boubert P, Cheron B, Addou A, Brisset JL (2002) Density and rotational temperature measurements of the NO° and OH° radicals produced by a gliding arc in humid air and their interaction with aqueous solutions. Plasma Chem Plasma Process 22:553–571
26. Brisset JL, Hnatiuc E (2012) Peroxynitrite: a re-examination of the chemical properties of non-thermal discharges burning in air over aqueous solution. Plasma Chem Plasma Process 32:655–674
27. Brisset JL, Moussa D, Doubla A, Hnatiuc E, Hnatiuc B, Kamgang YG, Herry JM, Bellon-Fontaine NM (2008) Chemical reactivity of discharges and temporal post-discharges in plasma treatment of aqueous media: examples of gliding arc discharge treated solutions. Ind Eng Chem Res 47:5761–5781
28. Brisset JL, Pawlat J (2015) Chemical effects of air plasma species on aqueous solutes in direct and delayed exposure modes: discharge, post-discharge and plasma activated water. Plasma Chem Plasma Process. doi:10.1007/s11090-015-9653-6
29. Hnatiuc E (2002) Procédés électriques de mesure et de traitement des polluants. Tech & Doc, Lavoisier, Paris
30. Djakaou I, Ghezzar RM, Zekri ME, Abdelmalek F, Cavadias S, Ognier S (2015) Removal of model pollutants in aqueous solution by gliding arc discharge. Part II: modeling and simulation study. Plasma Chem Plasma Process 35:143–157
31. Laminsi S, Acayanka E, Nzali S, Ndifon PT, Brisset JL (2012) Direct impact and delayed post-discharge chemical reactions of Fe^{II} complexes induced by non-thermal plasma. Deswater 37:38–45
32. Acayanka E, Laminsi S, Ndifon PT, Sop TB, Brisset JL (2013) Degradation of dithizone by non thermal quenched plasma of gliding arc type. J Adv Oxid Technol 16:188–197
33. Abia D, Nzali S, Acayanka E, Kamgang GY, Laminsi S, Ghogomu PM (2015) Synergetic effect of gliding arc discharge treatment and biosorption for removal of nitrophene and glycine from aqueous solution. J Ind Eng Chem 29:156–162
34. Djowe AT, Acayanka E, Lontio-Nkouongfo RG, Laminsi S, Gaigneaux EM (2015) Enhanced discolouration of Methyl Violet 10B in a gliding arc plasma reactor by the maghemite nanoparticles used as heterogeneous catalyst. J Environ Chem Eng 3:953–960
35. Laminsi S, Acayanka E, Ndifon PT, Tiya AD, Brisset JL (2012) plasmachemical dissociation and degradation of naphtol green B complex. Environ Eng Manag J 11:18–21
36. Tiya-Djowe A, Laminsi S, Noupeyi GL, Gaigneaux EM (2015) Non-thermal plasma synthesis of sea-urchin like α-FeOOH for the catalytic oxidation of Orange II in aqueous solution. Appl Catal B Environ 176:99–106
37. Yu J, Zhao X, Zhao Q (2000) Effect of surface structure on photocatalytic activity of TiO_2 thin films prepared by sol–gel method. Thin Solid Films 379:7–14
38. Jensen H, Soloviev A, Li Z, Sogaard EG (2005) XPS and FTIR investigation of the surface properties of different prepared titania nano-powders. Appl Surf Sci 246:239–249
39. Yu J, Su Y, Cheng B, Zhou M (2006) Effects of pH on the microstructures and photocatalytic activity of mesoporous nanocrystalline titania powders prepared via hydrothermal method. J Mol Catal A 258:104–112
40. Quan L, Xundao Y, Guangfu Z, Shiquan X (1997) Study on the microstructure and properties of nanosized stannic oxide powder. Mater Chem Phys 47:239–245
41. Radheshyam R, Senguttuvan TD, Lakshmikumar ST (2006) Study of the electric and optical bonding properties of doped SnO_2. Comput Mater Sci 37:15–19
42. Mountapmbeme-Kouotou P, Laminsi S, Acayanka E, Brisset JL (2013) Degradation of palm oil refinery wastewaters by non-thermal gliding arc discharge at atmospheric pressure. Environ Monit Assess 185:5789–5800
43. Liu Y, Xu H, Zhu S, Zhou M, Miao J (2014) Enhanced degradation of Acid Orange 7 solution by non-thermal plasma discharge with TiO_2. Plasma Chem Plasma Process 34:1403–1413
44. Saïm N, Ghezzar MR, Guyon C, Abdelmalek F, Tatoulian M, Addou A (2015) New prototype for the treatment of falling film liquid effluents by gliding arc discharge part II: plasmacatalytic activity of TiO_2 thin film deposited by magnetron Sputterin. Chem Eng Process 98:32–40